AGU PUBLICATIONS

JGR

Journal of Geophysical Research: Atmospheres

RESEARCH ARTICLE
10.1002/2015JD024404

Key Points:
- Widespread wintertime warm and cold extremes in Alaska were identified
- Atmospheric composites from 5 days before through the day of the extreme events were analyzed
- Temperature advection and anomalous longwave radiation were the primary factors for the extremes

Correspondence to:
J. J. Cassano,
john.cassano@colorado.edu

Citation:
Cassano, J. J., E. N. Cassano, M. W. Seefeldt, W. J. Gutowski Jr., and J. M. Glisan (2016), Synoptic conditions during wintertime temperature extremes in Alaska, *J. Geophys. Res. Atmos.*, *121*, 3241–3262, doi:10.1002/2015JD024404.

Received 27 OCT 2015
Accepted 12 MAR 2016
Accepted article online 19 MAR 2016
Published online 8 APR 2016

Synoptic conditions during wintertime temperature extremes in Alaska

John J. Cassano[1,2], Elizabeth N. Cassano[1], Mark W. Seefeldt[1], William J. Gutowski Jr.[3], and Justin M. Glisan[3]

[1]Cooperative Institute for Research in Environmental Sciences, University of Colorado Boulder, Boulder, Colorado, USA, [2]Department of Atmospheric and Oceanic Sciences, University of Colorado Boulder, Boulder, Colorado, USA, [3]Department of Geological and Atmospheric Sciences, Iowa State University of Science and Technology, Ames, Iowa, USA

Abstract The large-scale atmospheric state associated with widespread wintertime warm and cold extremes in southern Alaska was identified using 1989 to 2007 European Centre for Medium-Range Weather Forecasts Interim Re-Analysis (ERA-I) data. Extremes were defined as days with the coldest and warmest 1% of daily temperatures. Widespread extreme events were identified for days when at least 25 50 km grid cells in the study domain met the extreme temperature criteria. A total of 55 cold and 74 warm extreme days were identified in 19 winters. Composites of the atmospheric state from 5 days before through the day of the extreme events were analyzed to assess the large-scale atmospheric state associated with the extremes. The method of self-organizing maps (SOMs) was used to identify the range of sea level pressure (SLP) patterns present in the ERA-I December–February data, and these SLP patterns were then used to stratify the extreme days by their large-scale atmospheric circulation. Composites for all warm or cold extreme days showed less intense features than those for specific SLP patterns. In all of the composites temperature advection, strongest at 700 hPa, and anomalous longwave radiation were the primary factors that led to the extreme events. The anomalous downwelling longwave radiation was due to either reduced cloud cover, during cold extremes, or to increased cloud cover, during warm extremes. The SOM composites provided additional insight into the temporal evolution of the extreme days and highlighted different portions of southern Alaska most likely to experience temperature extremes for a given SOM SLP pattern.

1. Introduction

Extreme weather events can have a significant impact on society [*Intergovernmental Panel on Climate Change*, 2013]. Though global temperatures are broadly rising, this is occurring faster in the Arctic compared with the midlatitudes and tropics, a phenomenon known as Arctic amplification [*Serreze and Francis*, 2006; *Serreze et al*., 2009; *Screen and Simmonds*, 2010]. In addition to changes in mean temperatures, changes in temperature extreme events (hereafter extremes), particularly an increase in such events as heat waves and warm nights (with an associated decrease in cold extremes such as frost days), are expected to be observed as well [*Easterling et al*., 2000; *Tebaldi et al*., 2006; *Meehl et al*., 2009; *Horton et al*., 2015b; *Ning et al*., 2015]. Here we use the method of self-organizing maps (SOMs) [*Kohonen*, 2001] to characterize the large-scale atmospheric state associated with widespread wintertime daily temperature extremes in Alaska based on atmospheric reanalysis data. Identification of the relationship between extreme events and the large-scale atmospheric state allows analysis of extreme events in data sparse regions, such as the Arctic, using atmospheric reanalyses and for future climate change scenarios, using global climate models, since both reanalyses and global climate models are fairly skillful in reproducing the large-scale atmospheric circulation [*Randall et al*., 2007; *Flato et al*., 2013].

An overview of applying the SOM technique to climate data is provided by *Hewitson and Crane* [2002], while *Sheridan and Lee* [2011, and references therein] summarize the increasing body of literature that uses the SOM technique for atmospheric analysis and in the study of extremes. *Lennard and Hegerl* [2015] used a SOM framework to evaluate synoptic circulation patterns and rainfall, including extreme rainfall, in South Africa. *Horton et al*. [2015a] used the SOM technique to investigate recent trends in temperature extremes in the context of changing circulation patterns and found increases in circulation patterns conducive to both hot and cold extremes. *Loikith and Broccoli* [2015] evaluated circulation patterns associated with extreme daily temperature in climate models and observations and used a SOM analysis to evaluate differences between the two data sources.

Relating large-scale circulation and extremes has been used as an approach for many other studies. Here we provide a representative sample of these studies. *Kyselý* [2008] evaluated the importance of persistent circulation patterns on extremes in Europe and found positive (negative) radiation balance under high pressure or warm (cold) air advection to be important for warm (cold) extremes with persistent circulation patterns, slightly more important for warm extremes, enhancing the extremes severity. *Andrade et al*. [2012] studied the synoptic circulation associated with extremes in Europe and found warm and cold air advection important though the effect of cloudiness dampens the extremes. *Krueger et al*. [2015] performed composite analysis of temperature extremes in central Europe and found cold air advection, relative humidity, and radiation to be important for cold winter extremes. *Stefanon et al*. [2012] used a cluster analysis framework to evaluate heat waves in Europe and to investigate the physical mechanisms responsible for extremes associated with each cluster, while *Rodríguez-Puebla et al*. [2010] used an empirical orthogonal function framework to evaluate trends in warm days and cold nights on the Iberian Peninsula. *Ning and Bradley* [2015] used composite analysis to study the relationship between winter temperature and precipitation extremes in the northeastern United States and southeastern Canada and large-scale modes of climate variability (North Atlantic Oscillation, Pacific-North American pattern, and El Niño–Southern Oscillation). They found that pressure and associated wind anomalies explained the spatial patterns of temperature and precipitation extremes.

Some Arctic-focused studies of extremes include *Loikith and Broccoli* [2012] who evaluated composites of atmospheric circulation for temperature extremes over North America. For temperature extremes in eastern Alaska during January, they found circulation patterns that favored southerly (easterly) flow associated with warm (cold) air advection to be associated with warm (cold) extreme events. *Cassano et al*. [2006] evaluated temperature and wind extremes at Barrow, Alaska, during autumn using SOMs. They found that warm (cold) extremes were associated with southerly (northerly) flow. *Cassano et al*. [2011] also used SOMs to assess temperature anomalies associated with different sea level pressure patterns at several sites in Alaska but did not focus on extreme events. They found that warm temperature anomalies were generally associated with synoptic patterns that resulted in southerly flow, while cold anomalies were associated with northerly or easterly flow. *Cassano et al*. [2015] presented a framework for using SOMs to analyze extremes but focused primarily on issues related to training an appropriate SOM for analyzing extreme events and provided only brief examples of how SOMs could be used for analyzing extreme events.

The overarching goal of the current research is to identify and analyze the large-scale atmospheric state associated with widespread temperature extremes in Alaska using global atmospheric reanalysis data. This differs from the focus of *Cassano et al*. [2006, 2011], which analyzed the relationship between synoptic circulation and temperature at individual sites in Alaska rather than across broad regions. This work builds upon that presented in *Cassano et al*. [2015], using the same Alaska-focused SOM as that work, but provides a much more detailed analysis of the atmospheric state, including the atmospheric evolution in the days leading up to the extreme events, than *Cassano et al*. [2015]. Here composites of the atmospheric state for all warm and cold extremes will be compared to composites based on the SOM-identified large-scale circulation. Section 2 describes the data used for analysis as well as a description of extreme event definition, compositing, and SOM methodologies. Section 3 describes the large-scale atmospheric state associated with widespread warm and cold daily temperature extremes and compares composites for all cold and warm extreme days to SOM-based composites for both types of extremes. Section 4 contains a summary and conclusions.

2. Data and Methods

2.1. Data

We use data from the European Centre for Medium-Range Weather Forecasts' Interim Re-Analysis (ERA-I) [*European Centre for Medium-Range Weather Forecasts*, 2009; *Dee et al*., 2011] for December–February (DJF) 1989 to 2007 for the analysis presented here. Similar to its predecessor, ERA-40, ERA-I has been shown to be among the best global reanalyses for representing the Arctic atmosphere [*Lindsay et al*., 2014].

ERA-I daily averaged atmospheric state (sea level pressure (SLP), wind, and temperature) and surface fluxes (precipitation, downward longwave radiation (LWD), and downward shortwave radiation (SWD)) are interpolated to an equal area 50 km grid (Figure 1) and used for all subsequent analyses. Daily means of the state variables were calculated from the 00, 06, 12, and 18 UTC ERA-I analysis fields. The daily means for the flux variables were calculated from the daily accumulated fluxes (sum of 6-hourly accumulated fluxes at 06, 12,

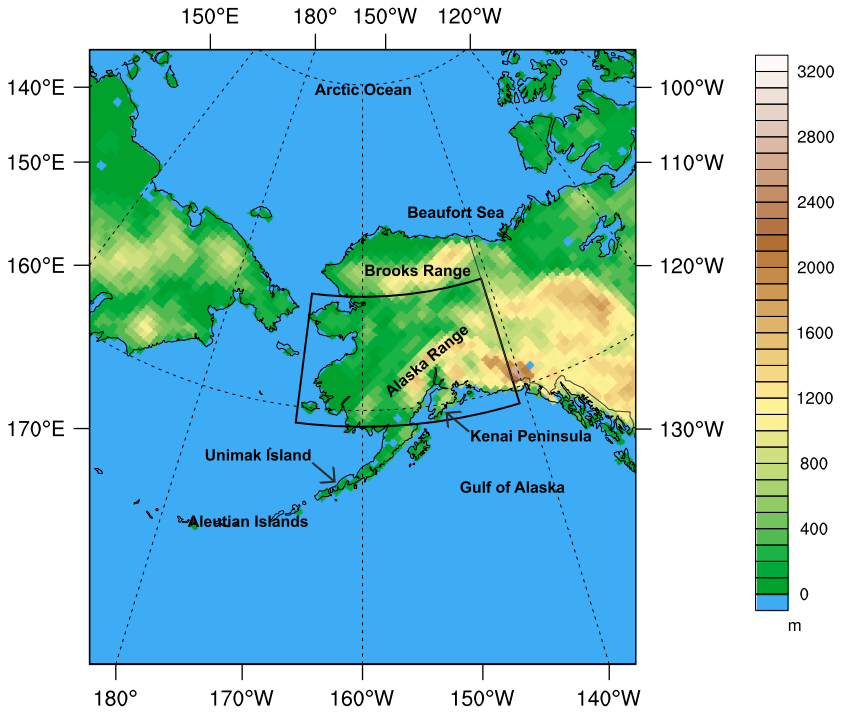

Figure 1. Topography of Alaska and surrounding regions. The black box indicates the region used to identify widespread extreme events. Place names referred to in the text are shown on the map.

and 18 UTC for the day of interest and 00 UTC for the following day) from the ERA-I forecast files. While some errors and biases in the reanalysis fields will exist the fact that all of the fields we analyze are from a physically consistent source allows us to explore the forcing mechanisms responsible for driving the extreme events depicted by the reanalysis.

Temperature extremes are defined using the ERA-I daily average 2 m temperature (T2m) data. Following *Cassano et al.* [2015], the SOM analysis of the large-scale near-surface circulation patterns was created using daily SLP spatial anomalies. SLP spatial anomalies were used as the basis for the SOM analysis because the SLP gradients, rather than absolute values of SLP, are responsible for determining the near-surface circulation and therefore are of most interest for this research. Daily SLP anomalies were calculated for each day by subtracting each day's domain-averaged SLP from the grid point values of SLP for the same day. SLP values from locations with elevation greater than 500 m were filtered out of the analysis due to errors associated with the reduction of surface pressure to SLP for high-elevation locations [*Wallace and Hobbs*, 1977; *Mohr*, 2004]. The SOM we use here is the same Alaska-focused SOM as used in *Cassano et al.* [2015].

2.2. Methodology

2.2.1. Definition of Extreme Events

Daily temperature extremes were identified in southern Alaska, largely south of the Brooks Range, excluding the Alaskan panhandle and most of the Aleutian Island chain (Figure 1). This analysis region is identical to the Alaska South region in *Cassano et al.* [2015]. This region was selected because the entire region will simultaneously be affected by a particular synoptic pattern [*Glisan and Gutowski*, 2014]. Only extremes over land grid points were considered for a total of 413 grid points in the study region.

Temperature extremes were defined using the same method as *Cassano et al.* [2015], and thus, our extreme events match those in *Cassano et al.* [2015]. Days exceeding the threshold of the coldest or warmest 1% of all days were identified at each grid point. If at least 25 grid points in the analysis region exceeded the warm or cold 1% threshold, this was deemed to be a widespread extreme day. Evaluating the data at each grid point individually allowed an analysis of the coldest/warmest conditions at a particular location rather than climatologically colder or warmer locations (e.g., northern (cold) or southern (warm) locations or regions favored

for cold or warm conditions due to the local topography). The analysis in this paper focuses on widespread extreme events, since these events are primarily controlled by the large-scale circulation that is well resolved in the reanalyses [*Randall et al*., 2007; *Flato et al*., 2013]. There was no requirement that the grid points be adjacent for a widespread extreme event, but the extreme grid points were either adjacent or in the same portion of the analysis region for most of the extremes analyzed.

2.2.2. Self-Organizing Maps

The large-scale near-surface circulation was classified using the SOM algorithm applied to daily SLP anomalies for DJF from 1989 to 2007 for a domain that was larger than the region used to identify widespread extremes (Figure 1). This larger domain was used to fully encompass the broad synoptic circulation that impacts the extremes region as discussed in *Cassano et al*. [2015].

Cassano et al. [2015] describe the SOM technique, but we include that description in the following paragraphs so that this critical aspect of the work is described fully in this paper. The SOM technique employs a neural network algorithm that uses unsupervised learning to determine generalized patterns in data and reduces the dimensions of large data sets by grouping similar data records together and organizing them into a two-dimensional array, referred to as a map or SOM. As a result, large, multidimensional data sets are reduced to more easily interpreted forms. Used in this way, the SOM algorithm may be considered a clustering technique, but unlike other clustering techniques, the SOM method does not need a priori decisions on data distribution and is instead trained through an iterative process. The final two-dimensional array of patterns (SOM) represents the full continuum of states represented in the training data set. This array is organized such that similar patterns are located in the same portion of the SOM with dissimilar patterns on opposite corners of the array. This organization of the final patterns allows for easier analysis of interpattern relationships and allows adjacent patterns to be grouped together to analyze the behavior of subsets of the entire SOM space. *Kohonen* [2001] provides a detailed description of the SOM algorithm, and *Hewitson and Crane* [2002] provide additional information on the application of the SOM technique to climate data.

Cassano et al. [2015] review many of the issues that need to be considered when using the SOM technique. A critical decision that needs to be made when applying the SOM technique is the number of patterns to be defined by the algorithm. The advantage of using a relatively small number of patterns is that clearly distinguishable differences in features can be seen in each pattern and a relatively small SOM is easy to visualize. The disadvantage of using a small number of patterns is that each pattern can become too generalized and not allow for clear identification of features relevant to relatively rare events. The use of larger SOM arrays provides for finer differences between each pattern and can help separate patterns with relatively similar features but important small-scale differences. The disadvantages of using a large SOM array include difficulty in visualizing all of the patterns and issues of representativeness of the patterns caused by the small numbers of events corresponding to each pattern. Many previous SOM-based atmospheric studies have used a 7×5 (35 patterns) SOM, and for this work we also use a 7×5 SOM that balances the advantages and disadvantages of smaller or larger SOMs. *Cassano et al.* [2015] discuss the choice of a 7×5 SOM for the analysis of Alaskan temperature extremes in greater detail. One key result in their work was that use of a smaller 5×4 SOM resulted in significant overlap of warm and cold extremes on individual SOM patterns, and they suggest that this indicates that a 5×4 SOM is too small for the study of temperature extremes.

The SOM used here identifies the range of SLP anomaly patterns present in winter in the vicinity of Alaska and is the same one used in *Cassano et al.* [2015] (Figure 2). The SLP anomaly patterns include low pressure near the western end of the Aleutian Islands (left side of SOM), low pressure centered in the Gulf of Alaska (bottom right corner of the SOM), and low pressure to the north over the Bering Sea or Arctic Ocean (top right). High pressure located over the Arctic Ocean is found in most of the SOM patterns except a few on the right side of the SOM. The Arctic high pressure can extend across Alaska and into the Gulf of Alaska (left side of the SOM) or can extend south over eastern Siberia (bottom right and bottom center of the SOM). Patterns in the top right corner of the SOM are dominated by high pressure in the North Pacific and the Gulf of Alaska rather than by high pressure in the Arctic Ocean.

Once the SOM has been defined, individual daily SLP anomaly fields can be mapped to the SOM by associating each daily SLP sample with a single pattern on the SOM. This is accomplished by identifying the SOM pattern that has the minimum squared difference in SLP anomaly with the daily SLP sample of interest. By repeating this mapping for all of the samples in the data set, a list of samples associated with each SOM

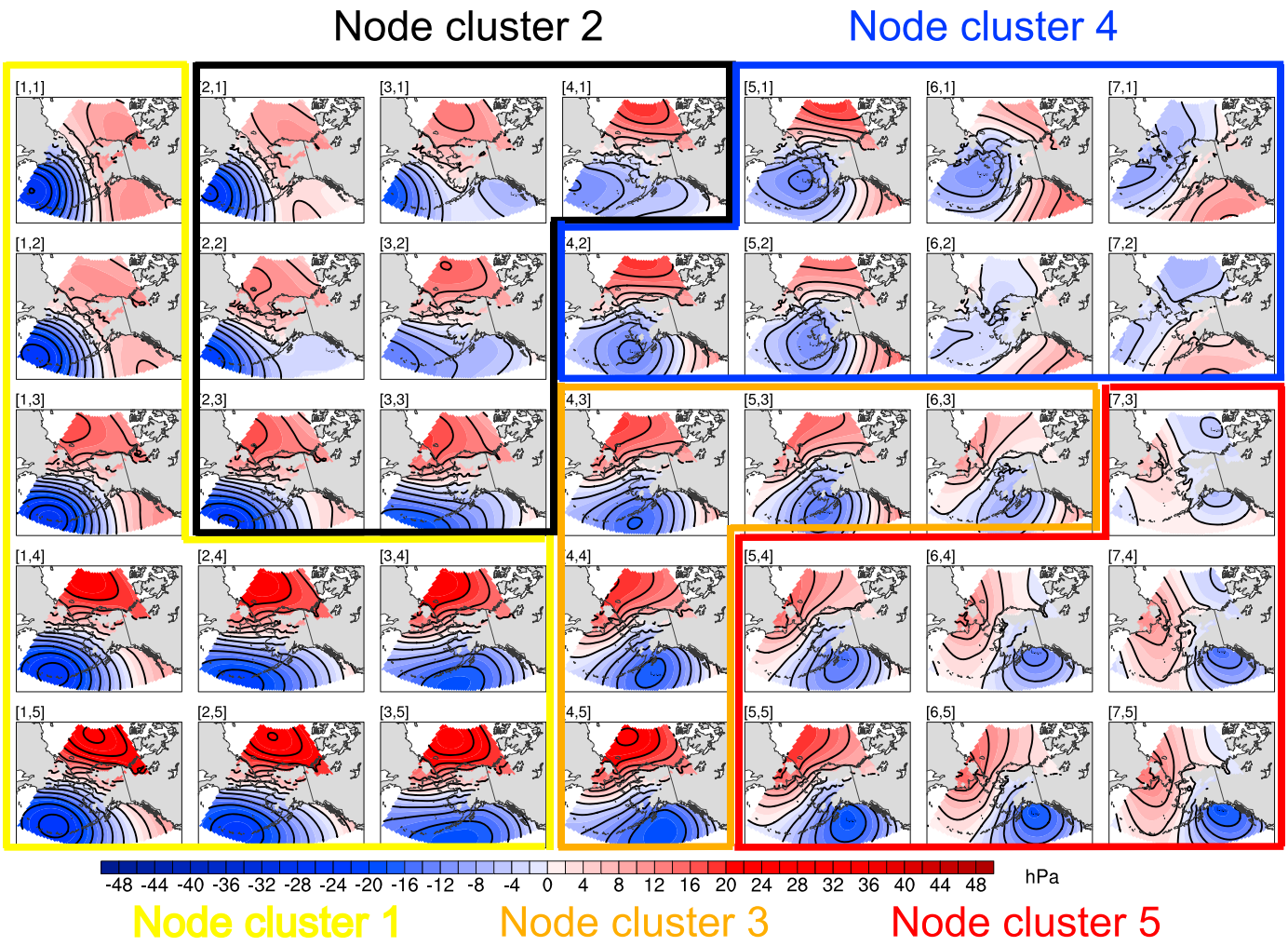

Figure 2. SOM of SLP anomalies. Node clusters are shown by colored outlines, and the definition of these clusters is discussed in the text and Table 2. (modified from *Cassano et al.* [2015]).

pattern is created. The list of samples associated with each pattern can be used with the list of widespread extreme days to identify which SOM patterns are associated with warm or cold extremes. One can thus obtain a frequency distribution in the SOM array for climatology (all daily SLP anomalies) and for the widespread warm or cold extremes.

2.2.3. Composites

Composites of the atmospheric state and fluxes were calculated for the extreme events by averaging any ERA-I variable of interest for all days when a particular type (warm or cold) of widespread extreme event occurred. Composites for nonextreme days were calculated in a similar manner. Differences between the extreme and nonextreme composites highlight how the atmospheric state differs between extreme and nonextreme days. The statistical significance of the difference between extreme and nonextreme composites was calculated using a standard *t* test and a 95% significance level.

The list of days associated with each SOM pattern was also used to create composites for warm, cold, and nonextreme days for each SOM pattern. Unlike the composites for all extreme days the SOM composites are representative of only those extremes that occur for a particular type of SLP pattern. These SOM composites have the advantage that they do not average out potentially important differences since they are created for a single SLP pattern type rather than for the range of SLP patterns encompassed by all extreme events. The SOM composites are compared with more general composites of all warm or cold extreme events in the section 3.

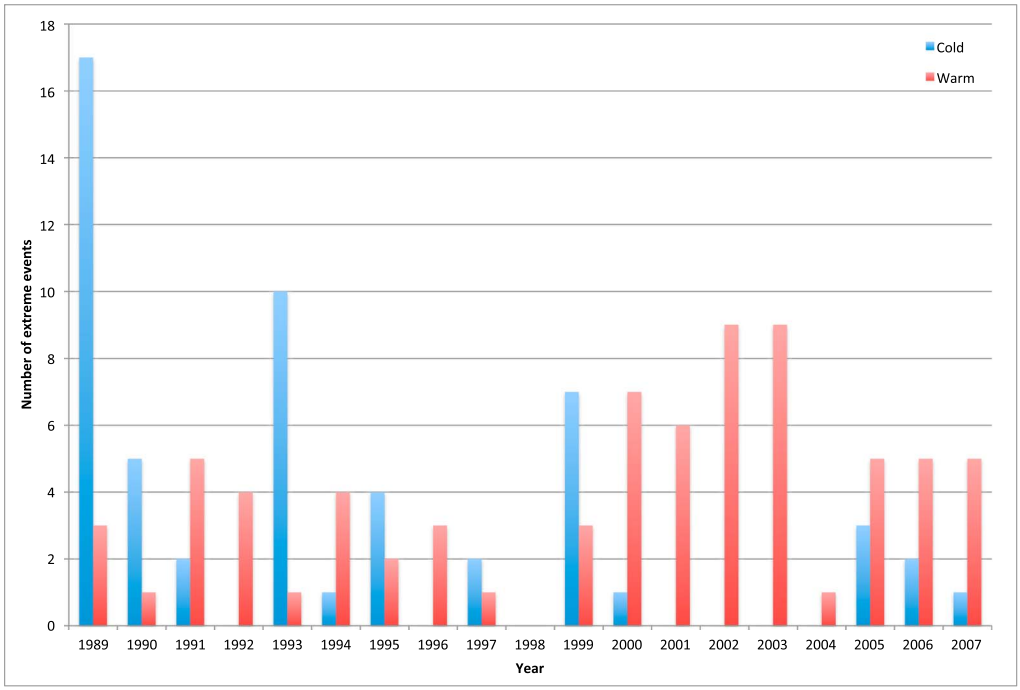

Figure 3. Number of widespread cold and warm extreme days per year from 1989 to 2007.

To assess the temporal evolution of the atmosphere prior to the occurrence of widespread extreme days, composites for all days prior to a given type of extreme day were calculated for 1 to 5 days prior to the extreme day occurrence. These composites will be referred to as day-5 to day-1 composites. It should be noted that the days that comprise the day-5 to day-1 composites may or may not be extreme days themselves. Further, as discussed below, these days may or may not occur in the same SOM cluster as the extreme days (see section 3.3).

Rather than creating composites based on the days prior to individual extreme days, it would also be possible to create composites for extreme events, with events being defined as multiple consecutive extreme days. While this compositing strategy would potentially avoid having extreme days included in the day-5 to day-1 composites, it was felt that day-based compositing, rather than event-based compositing, provides the most easily interpreted representation of the atmospheric state prior to a given extreme day and avoids issues related to how to define extreme events that consist of multiple extreme days, possibly separated by a small number of nonextreme days. While the day-based composites presented below include some extreme days as part of the day-5 to day-1 composites, this was deemed appropriate and desirable, as it highlights the persistence of the atmosphere present in some of the extreme day events.

3. Results

3.1. Overview of Widespread Extreme Events

Using the definition of widespread extreme events presented in section 2.2.1, a total of 55 cold extreme days and 74 warm extreme days were identified during the winters of 1989 to 2007 (Figure 3 and Table 1). As seen in Figure 3, the majority of the cold extreme days occur prior to 1998, while the majority of warm extreme

Table 1. Number of Extreme Days (Second Column), Single-Day Events (Third Column), All Multiday Events (Fourth Column), and Events Lasting Four or More Days (Fifth Column)[a]

Extreme Type	Extreme Days	Single-Day Events	Multiday Events	Long Events
DJF cold	55	7 (12.7%)	10 (87.3%)	6 (72.0%)
DJF warm	74	23 (31.1%)	17 (68.9%)	3 (27.0%)

[a]Numbers in parentheses indicate the percent of all extreme days that occur for the events of a given duration.

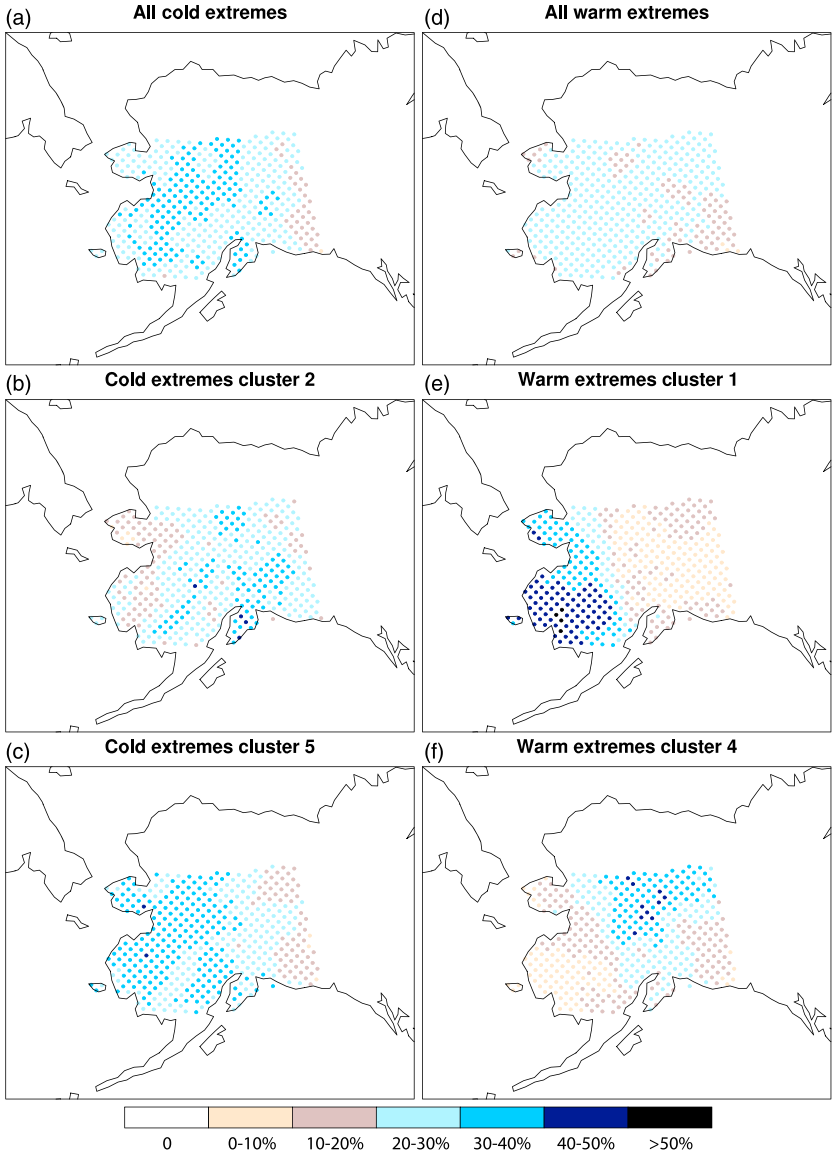

Figure 4. Percent of all widespread extreme days that occur at each grid point in the southern Alaska analysis region for (a) all 55 cold extreme days, (b) the 21 cold extreme days associated with SOM cluster 2, (c) the 28 cold extreme days associated with SOM cluster 5, (d) all 74 warm extreme days, (e) the 32 warm extreme days associated with SOM cluster 1, and (f) the 29 warm extreme days associated with SOM cluster 4.

days occur after 1998. The number of extreme days per year also varies from 0 to 17 (9) for cold (warm) extremes. A large fraction of the extreme days, 87.3% of cold and 68.9% of warm, occurred as part of a multiday event (Table 1). Long events were defined as those that occurred for four or more consecutive days. Cold extremes were much more likely to occur as part of long-duration extreme events (72%) compared to warm extremes (27%) (Table 1). These statistics suggest that once conditions favoring the formation of a widespread extreme occur, these events are able to persist for multiple days, particularly in the case of cold extremes.

For each grid point the number of days identified as being part of either a warm or cold widespread extreme is calculated, and this is presented in Figures 4a and 4d as the percent of all extreme days (55 for cold extremes and 74 for warm extremes). The warm extremes occurred with relatively uniform frequency across the study domain other than a slight reduction in extreme event frequency near the eastern edge of Alaska (Figure 4d). The cold extremes showed a more spatially heterogeneous pattern with a preference for cold

extremes from the north central to the southwest portion of the study domain (Figure 4a). This preferred location for cold extremes is north and west of the high terrain of the Alaska Range (Figure 1), and the preference for cold extremes in this region may reflect the shallow nature of extremely cold air masses and that these very cold air masses, which originate to the north, often cannot cross the high terrain of the Alaska Range.

3.2. Composites of All Warm and Cold Extremes

One approach for analyzing the synoptic setting of extreme events is to create composite plots of all events of a given extreme type [e.g., *Goyette*, 2011; *Metz et al*., 2013; *Cassano et al*., 2015; *Grotjahn et al*., 2015]. Figures 5 and 6 show composites of selected variables (SLP, T2m, 10 m wind, 700 hPa temperature (T700) and wind, and anomalies of LWD) for all widespread cold and warm extremes, respectively, for days prior to and including the extreme event day. The LWD anomalies are calculated as the difference between the average LWD for a given type of extreme (warm or cold) and the average LWD for all nonextreme days. These plots reveal clearly different synoptic conditions for cold and warm extremes as would be expected.

For the cold extremes the SLP composite (Figure 5, first column) at day-5 shows a surface low located in the Gulf of Alaska with high pressure over far eastern Siberia. The surface low intensifies by day-3 and then gradually weakens by the time the extreme day occurs. During this time the high pressure in Siberia strengthens and expands eastward covering most of Alaska by the extreme day. The high pressure and adjacent regions are consistently significantly different in the extreme composite compared to the nonextreme composite (stippling in Figure 5) indicating that the high pressure is the main SLP feature that distinguishes the extreme from nonextreme days. Significant differences near the center of the high-pressure center indicate that the intensity of the high is significantly different from the nonextreme days, while significant differences on the periphery of the high-pressure center indicate that the high is larger in the extreme than nonextreme day composites. This applies to both high- and low-pressure centers in all of the composites shown below. This synoptic pattern results in northerly surface flow over much of Alaska that weakens as the high builds over Alaska and the pressure gradient over the state slackens (Figure 5, second column). During the 5 days leading up to the extreme day the coldest T2m moves from over the North Slope of Alaska to central Alaska with the temperature of the surface air mass falling during this period (Figure 5, second column). The surface winds and T2m suggest that cold air is advected south over Alaska but that this air mass is modified, becoming colder over time. The flow and temperature evolution at 700 hPa is similar to that at the surface (Figure 5, third column) except that the coldest air originates over the Arctic Ocean and slowly moves south to north central Alaska by the extreme days. This evolution suggests that cold air advection dominates at 700 hPa given the movement of the coldest air in a direction consistent with the winds at this level and because there is little change in the coldest temperatures present. The cooling with time of the surface air mass is driven by negative anomalies in LWD relative to the nonextreme days (Figure 5, fourth column). These LWD anomalies become increasingly negative with time falling to values less than $-70\,\mathrm{W\,m^{-2}}$ by the extreme day and are statistically different from the nonextreme composite LWD anomalies over all of Alaska for all days leading up to the extreme event.

The dominant SLP feature for the warm extreme days is low pressure over the Aleutian Islands with high pressure over western Canada and north of Alaska (Figure 6, first column). Both of these features are significantly different in the extreme and nonextreme composites for all days leading up to the extreme event. This sea level pressure pattern results in broad southerly flow over Alaska originating over the Pacific Ocean. During the 5 days leading up to the warm extreme events warm air is advected north over the Pacific Ocean (most evident between day-5 and day-3) with this warm air spreading over Alaska over time (Figure 6, second column). A strong temperature gradient exists along the southern Alaska coast as a result of the relatively warm ocean temperatures compared to the colder, typically snow-covered land surface. This snow-covered surface limits the amount of warming possible over Alaska despite the fact that warm air advection is occurring. The warm air advection associated with this synoptic setting is more clearly displayed at 700 hPa (Figure 6, third column). At this level the northward advance of warm air from the North Pacific over Alaska is evident from day-5 through the warm extreme day. Positive LWD anomalies that are statistically significant over much of Alaska for the days leading up to and including the warm extreme day contribute to warming the lower atmosphere, with maximum anomalies in excess of $+70\,\mathrm{W\,m^{-2}}$.

The cold and warm extreme composites (Figures 5 and 6) identify the different synoptic conditions that lead to warm and cold extremes in Alaska. Both sets of composites highlight the role of temperature advection in

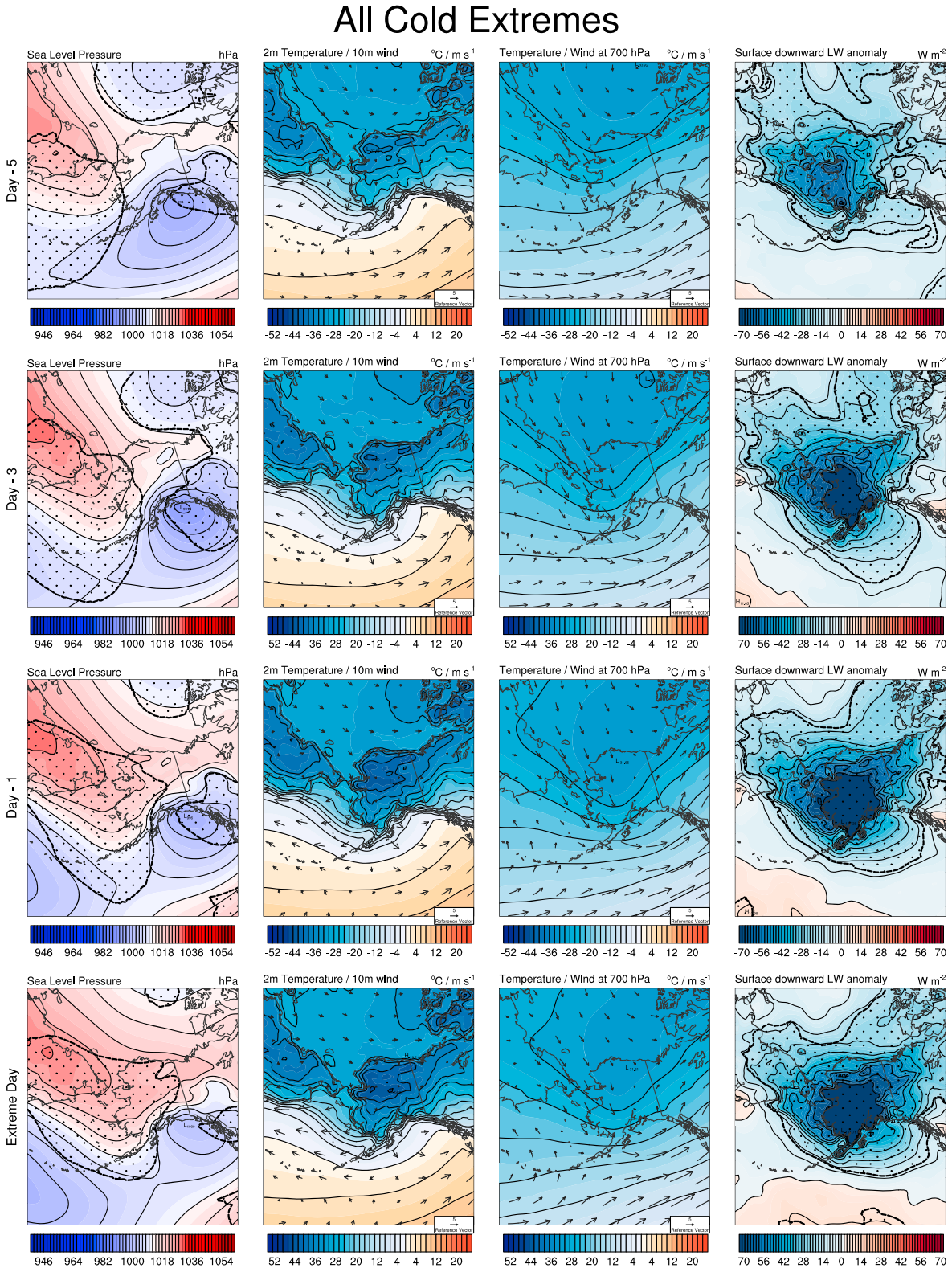

Figure 5. Composite for all widespread cold extreme days of (first column) sea level pressure (SLP), (second column) 2 m air temperature (T2m) and 10 m wind, (third column) 700 hPa temperature (T700) and wind, and (fourth column) difference between extreme day and nonextreme day downward longwave radiation at the surface (LWD). Composites are for (first row) 5 days (day-5), (second row) 3 days (day-3), and (third row) 1 day (day-1) prior to the extreme day and (fourth row) the extreme day. Stippling indicates locations where the difference between the extreme day and nonextreme day composites differs at the 95% significance level based on a standard *t* test.

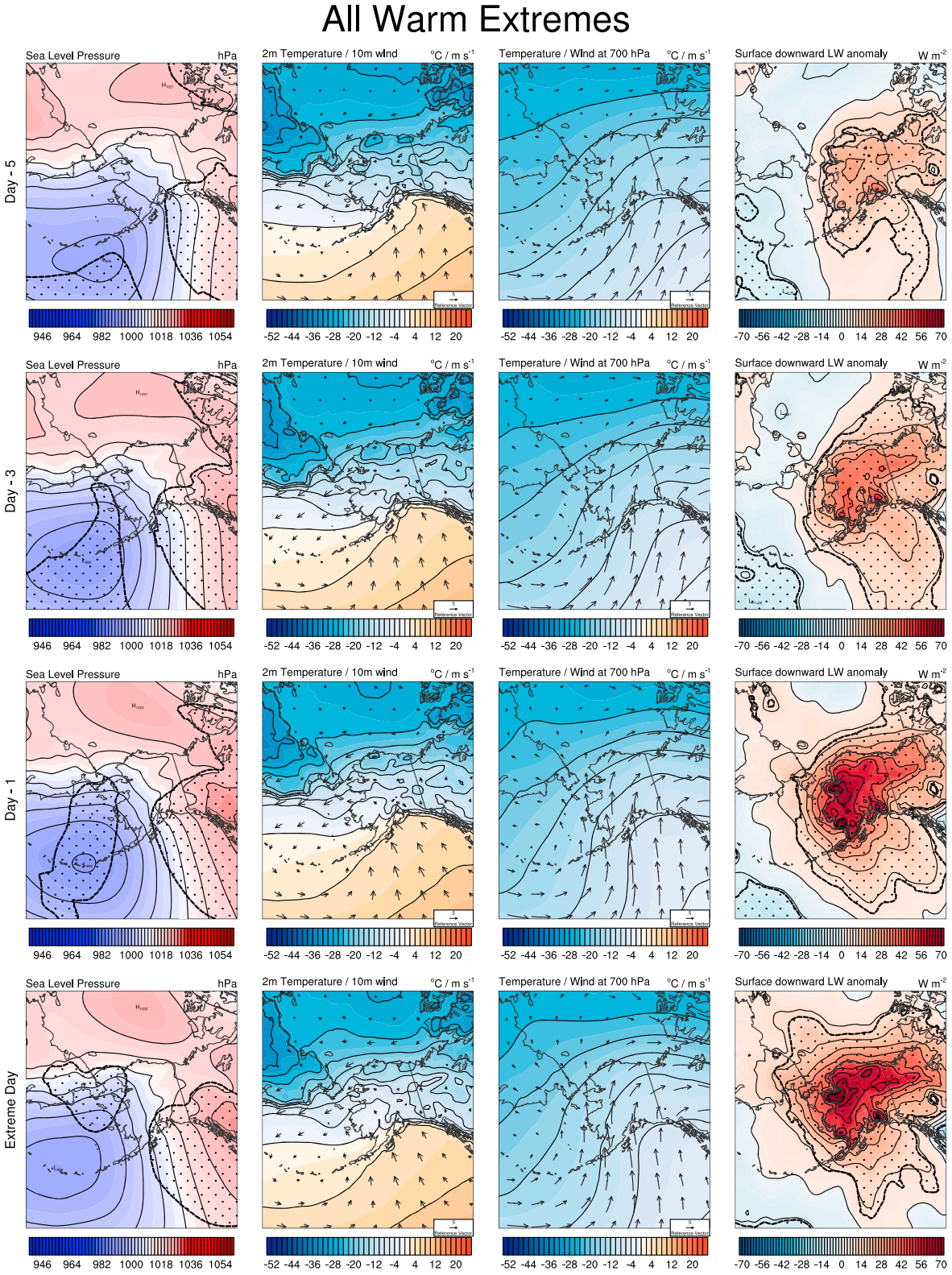

Figure 6. Composite for all widespread warm extreme days of (first column) sea level pressure (SLP), (second column) 2 m air temperature (T2m) and 10 m wind, (third column) 700 hPa temperature (T700) and wind, and (fourth column) difference between extreme day and nonextreme day downward longwave radiation at the surface (LWD). Composites are for (first row) 5 days (day-5), (second row) 3 days (day-3), and (third row) 1 day (day-1) prior to the extreme day and the (fourth row) extreme day. Stippling indicates locations where the difference between the extreme day and nonextreme day composites differs at the 95% significance level based on a standard *t* test.

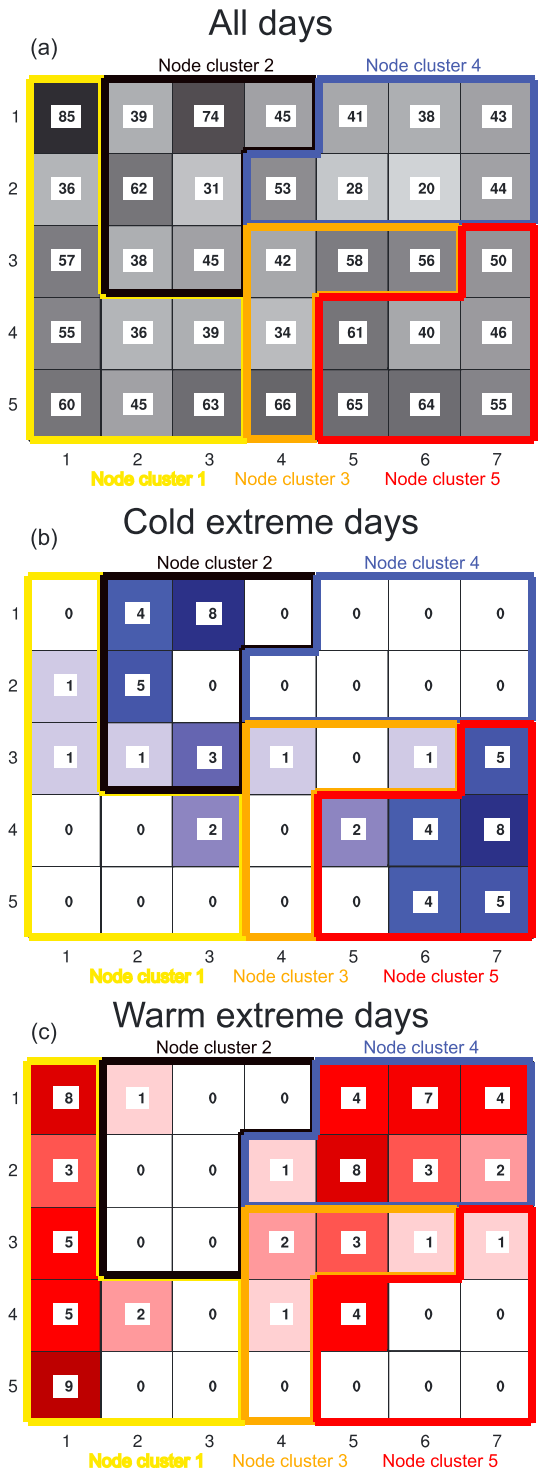

Figure 7. Number of days that map to each SOM pattern for (a) all DJF days, (b) all cold extreme days, and (c) all warm extreme days. Darker shading (gray = all DJF days, blue = all cold extreme days, and red = all warm extreme days) indicates a greater number of days mapping to a given SOM pattern. Node clusters are shown by colored outlines, and the definition of these clusters is discussed in the text and Table 2. (modified from *Cassano et al.* [2015]).

driving the extreme events, with the advection being most clearly shown above the surface (700 hPa). Radiative forcing modifies the air mass over time leading up to the extreme days. This is most obvious for the cold extremes as the minimum air mass temperature decreases with time, as cold air is advected into the extremes study region. In contrast, the snow-covered land surface cools the northward advected warm air near the surface for the warm extremes. Despite the unique large-scale features identified for the warm and cold composites, it is likely that more subtle differences in synoptic setting for the extremes are present and that some of these features may be masked by compositing all of the warm or cold extreme events together.

3.3. SOM-Based Analysis of Warm and Cold Extremes

The synoptic patterns identified by the SOM algorithm (Figure 2) can be used to identify the range of synoptic conditions associated with either warm or cold extreme days. The number of days that map to each SOM pattern for all DJF days is shown in Figure 7a, while the number of days that map to each SOM pattern for just the cold and warm extreme DJF days are shown in Figures 7b and 7c, respectively. The portion of SOM space in which warm and cold extremes occur is largely distinct, with only a few SOM patterns associated with both warm and cold extremes. Further, the distribution of either warm or cold extremes across SOM space is distinct from that for all DJF days. The probability that the cold or warm extreme days would fall only on the SOM patterns shown in Figures 7b and 7c is very low [*Cassano et al.*, 2015] indicating that this distribution of extreme events across the SOM space does not occur by chance and instead indicates that there are preferred portions of SOM space in which warm or cold extremes occur.

The cold extremes tend to occur mainly in the lower right and near the top left corners of the SOM. These two portions of the SOM space are characterized by low pressure in the Gulf of Alaska with high pressure over eastern Siberia and north of Alaska (lower right corner) or with high pressure located over Alaska and low pressure in the far western portion of the domain (top left portion of SOM) (Figures 2 and 7b). In contrast, the warm extremes tend to be associated with synoptic patterns in the top right corner and along the left edge of the SOM. Both of these portions of the SOM space are characterized by SLP patterns with low pressure to the west and high pressure to the east of Alaska (Figures 2 and 7c).

Table 2. Characteristics Used to Define SOM Node Clusters

Cluster Number	Cluster Name: Characteristics
1	Aleutian Low: Center of low west of Unimak Island
2	Transitional: Aleutian Low that may also have a secondary low or trough in the Gulf of Alaska
3	Eastward shifted Aleutian Low: Center of low east of Unimak Island and west of Kenai Peninsula
4	Bering/Arctic low: Center of low located in Bering Sea or Arctic Ocean
5	Gulf of Alaska low: Center of low east of Kenai Peninsula

Previous SOM-based analyses have found that grouping adjacent SOM patterns is useful for identifying more generalized patterns relative to the individual SOM patterns [e.g., *Leloup et al*., 2007, 2008; *Finnis et al*., 2009; *Seefeldt and Cassano*, 2012; *Nigro and Cassano*, 2014a, 2014b; *Mills and Walsh*, 2014; *Shan et al*., 2014; *DuVivier and Cassano*, 2015]. Table 2 lists low-pressure center locations that were used to subjectively define five clusters in the SOM. Changes in the position of the primary low-pressure center within each SOM pattern will alter the large-scale flow over the Alaskan study domain and could impact the occurrence of warm or cold extremes. It should be noted that these clusters were defined without reference to the number of warm and cold extreme days that map to each SOM pattern, but only two clusters are associated with the vast majority of the cold (warm) extremes (Table 3). Almost 90% of the cold extremes are associated with SOM patterns in clusters 5 (50.9%) and 2 (38.2%), while over 80% of the warm extremes are associated with SOM patterns in clusters 1 (43.2%) and 4 (39.2%). The fact that the cold (warm) extremes cluster in two distinct portions of the SOM space indicates that there are distinct synoptic patterns associated with different cold (warm) extremes. We take advantage of this distinct separation of extremes across SOM space to provide a more detailed composite analysis of the large-scale setting and forcing for cold and warm extremes.

3.3.1. SOM-Based Composites of Cold Extremes

The cold extremes associated with SOM cluster 5 account for the majority of all cold extremes (50.9%). These extreme events occur mainly in the western portion of the analysis domain (Figure 4c). The location of the surface low- and high-pressure centers associated with this cluster is relatively unvarying from day-5 to the extreme day with low pressure in the Gulf of Alaska and over the northern Beaufort Sea and high pressure over eastern Siberia extending across northern Alaska (Figure 8, first column). The Gulf of Alaska low strengthens slightly between day-5 and day-1 and becomes significantly different from the nonextreme composite by the extreme day. The high pressure over Siberia becomes significantly different from the nonextreme composite by day-3, while the low pressure north of Alaska, in the Beaufort Sea, is significantly different from the nonextreme composite for all days leading up to the extreme event. The surface winds over Alaska (Figure 8, second column) are mainly northeasterly at day-5, shift to northerly by day-3, and weaken over time leading up to the extreme day. The weak northeasterly to northerly flow drives weak cold air advection, while the weakening winds with time likely allow strong surface-based inversions to develop as the extreme day approaches. While some evolution of the SLP and wind fields is evident from day-5 to day-1, the SLP pattern shown in these composites is relatively stationary. Of the 28 days that map to cluster 5 12 of the day-5, 19 of the day-3, and 20 of the day-1 days map to SLP patterns in cluster 5 (not shown).

At day-5 the coldest T2m is located over the North Slope of Alaska and Siberia (Figure 8, second column). The coldest air expands southward over Alaska from day-5 to the extreme day with T2m steadily decreasing over the study domain with time. The movement of the coldest air south suggests that cold air advection is occurring, while the decreasing temperature of the coldest air indicates diabatic processes modifying this air mass over time. The temporal evolution of the T700 field is similar to that of T2m except that the coldest T700 is located over the northern Beaufort Sea at day-5. This cold air spreads south in the days leading up to the extreme event, consistent with the northerly 700 hPa flow. T700 also decreases with time indicating that air mass modification as well as temperature advection is occurring although the air mass modification at this level is less pronounced than at the surface. Based on the T2m and T700 evolution, it appears that air mass modification dominates the T2m changes while advection dominates T700. Composite

Table 3. Number and Percent of All Cold (Second Column) and Warm (Third Column) Widespread Extremes in Each SOM Cluster

Cluster Number	Cold Extremes	Warm Extremes
1	4 (7.2%)	32 (43.2%)
2	21 (38.2%)	1 (1.4%)
3	2 (3.6%)	7 (9.5%)
4	0 (0.0%)	29 (39.2%)
5	28 (50.9%)	5 (6.8%)

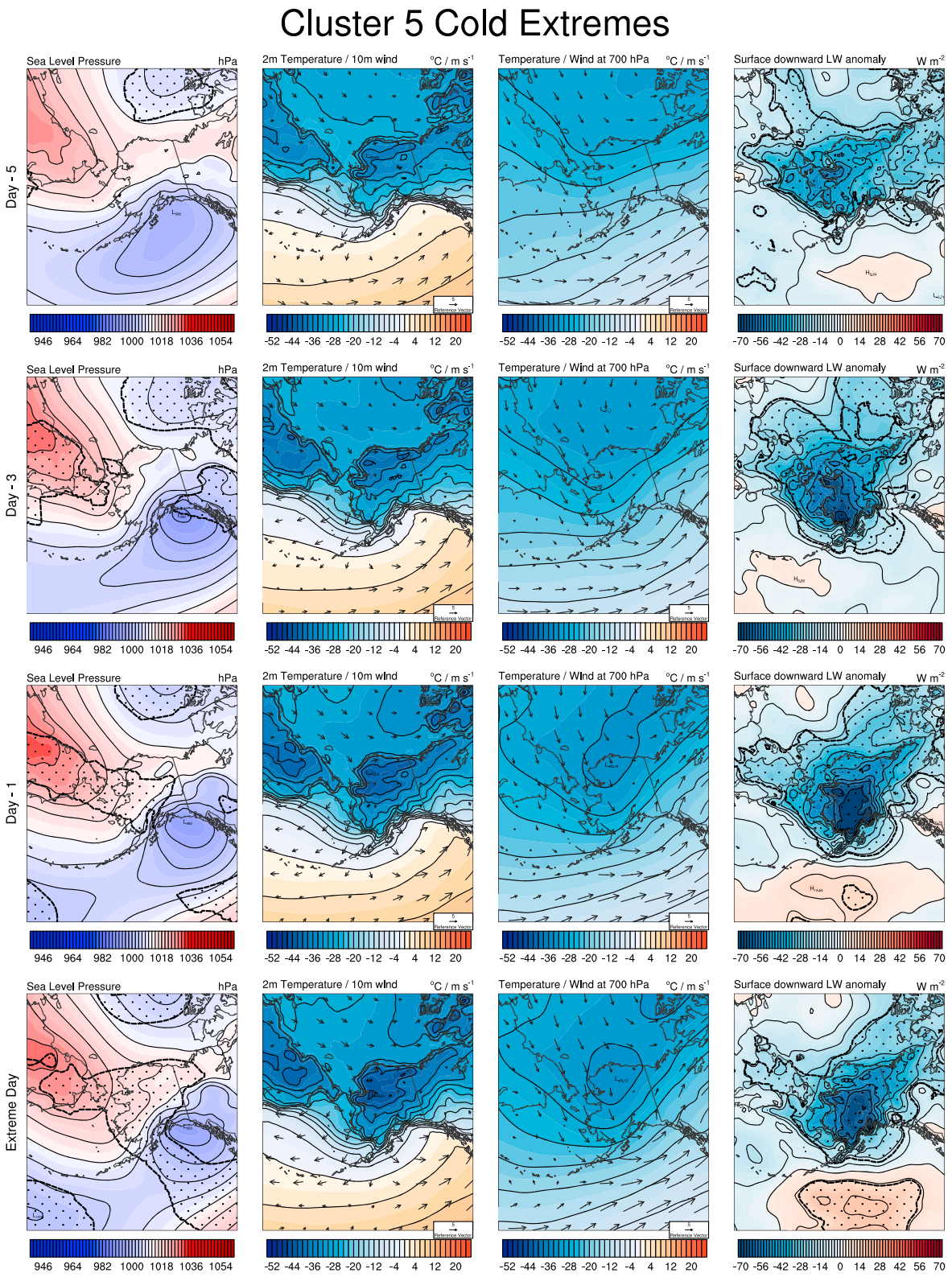

Figure 8. Composite for all widespread cold extreme days mapping to SOM cluster 5 of (first column) sea level pressure (SLP), (second column) 2 m air temperature (T2m) and 10 m wind, (third column) 700 hPa temperature (T700) and wind, and (fourth column) difference between extreme day and nonextreme day downward longwave radiation at the surface (LWD). Composites are for (first row) 5 days (day-5), (second row) 3 days (day-3), and (third row) 1 day (day-1) prior to the extreme day and the (fourth row) extreme day. Stippling indicates locations where the difference between the extreme day and nonextreme day composites differs at the 95% significance level based on a standard *t* test.

LWD anomalies, relative to the nonextreme DJF days, are negative and significant over all of Alaska from day-5 to the extreme day with the negative anomalies increasing in magnitude over time (Figure 8, fourth column). These negative LWD anomalies contribute to cooling the lower atmosphere. SWD anomalies (not shown) are weaker than the LWD anomalies but are of opposite sign indicating that the radiative anomalies are driven by anomalously clear skies. These clear skies are associated with anomalously low column-integrated water vapor amounts (not shown).

The cold extremes associated with SOM cluster 2 (38.2% of all cold extremes) occur across the entire analysis domain with increased frequency in the southern and north central portion of the domain (Figure 4b). At day-5 the SLP field is characterized by high pressure over Siberia and low pressure centered in the northern Gulf of Alaska (Figure 9, first column). Significant differences in the SLP anomaly between the extreme and nonextreme days at day-5 are found south of the Siberian high and centered on and north of the Gulf of Alaska low. Over the next 5 days the high pressure moves east over Alaska and strengthens, while the low in the Gulf of Alaska remains stationary and weakens. The primary region of significant SLP differences between the extreme and nonextreme days from day-3 to the extreme day is centered on the high-pressure region, indicating the importance of this high in forcing the extremes. This SLP pattern drives northerly winds over most of Alaska, strongest over western Alaska at day-5 (Figure 9, second column). These surface winds weaken as the extreme day approaches, as a result of the light pressure gradient associated with the high-pressure building over Alaska.

At day-5 the coldest T2m is located in Siberia and over far northern Alaska (Figure 9, second column). The cold air in Alaska spreads south and becomes colder leading up to the extreme day. Similar to cluster 5, it appears that weak cold air advection is occurring, but much of the T2m change with time is driven by diabatic processes. At 700 hPa the coldest air at day-5 is located north of Alaska over the Beaufort Sea (Figure 9, third column). This cold air moves south with time, consistent with the northerly flow at 700 hPa. Unlike at the surface the coldest air at 700 hPa does not cool and, in fact, even warms slightly as the extreme day approaches. At 700 hPa cold air advection dominates the temperature changes over the study domain, and if anything, weak diabatic warming of the air mass occurs in the days immediately leading up to the extreme event at this level. As was found for the cluster 5 composites, a significant negative LWD anomaly persists and strengthens over Alaska from day-5 to the extreme day (Figure 9, fourth column) leading to anomalous cooling of the near-surface air. This negative LWD anomaly is collocated with a weaker positive SWD anomaly (not shown) indicating that the radiative anomalies are driven by anomalously clear skies. Anomalously low column-integrated water vapor amounts (not shown) combined with a 500 hPa ridge building over the Bering Sea (not shown) both likely contribute to the anomalously clear skies.

Comparison of the cold extreme composites for all cold extreme days (Figure 5), the cluster 5 cold extreme days (Figure 8) and the cluster 2 cold extreme days (Figure 9) reveal some similarities in the synoptic setting responsible for these three sets of cold extremes. In all three cases the day-5 SLP field is characterized by high pressure over Siberia with low pressure in the Gulf of Alaska. For cluster 5 the low- and high-pressure centers remain relatively stationary with little change in intensity over time, while for cluster 2 the high pressure expands over Alaska, while the Gulf of Alaska low weakens with time. As would be expected, the all cold extremes composite shows a mix of these features. In all three cases cold air advection, most evident above the surface at 700 hPa, combined with strong radiative cooling of the surface (as shown by negative LWD anomalies), contribute to the development of the extreme cold T2m. In all cases the strong radiative cooling occurs in response to reduced cloud cover. The surface winds weaken from day-5 to the extreme day indicating that advection becomes less important as the extreme day approaches. The light winds occurring during the extreme day allow strong surface-based inversions to develop enhancing the cooling occurring immediately adjacent to the surface. The location of the most frequent cold extremes differs between clusters 2 and 5 and is the most notable difference between the cold extremes for these two clusters. The cold extremes in cluster 2 are spread almost uniformly across the study domain, while for cluster 5 the cold extremes occur preferentially in the western part of the study domain. The different locations of the cold extremes reflect the different SLP evolution for these two clusters. The large high-pressure spreading across northern and central Alaska in cluster 2 favors cold extremes across all of southern Alaska, while the more westerly position of the high pressure in cluster 5 favors a more westerly location of the cold extremes.

As mentioned in section 2.2.3, because the day-5 to day-1 composites are calculated relative to individual extreme days and because many of the cold extremes are long events of more than 4 days in duration

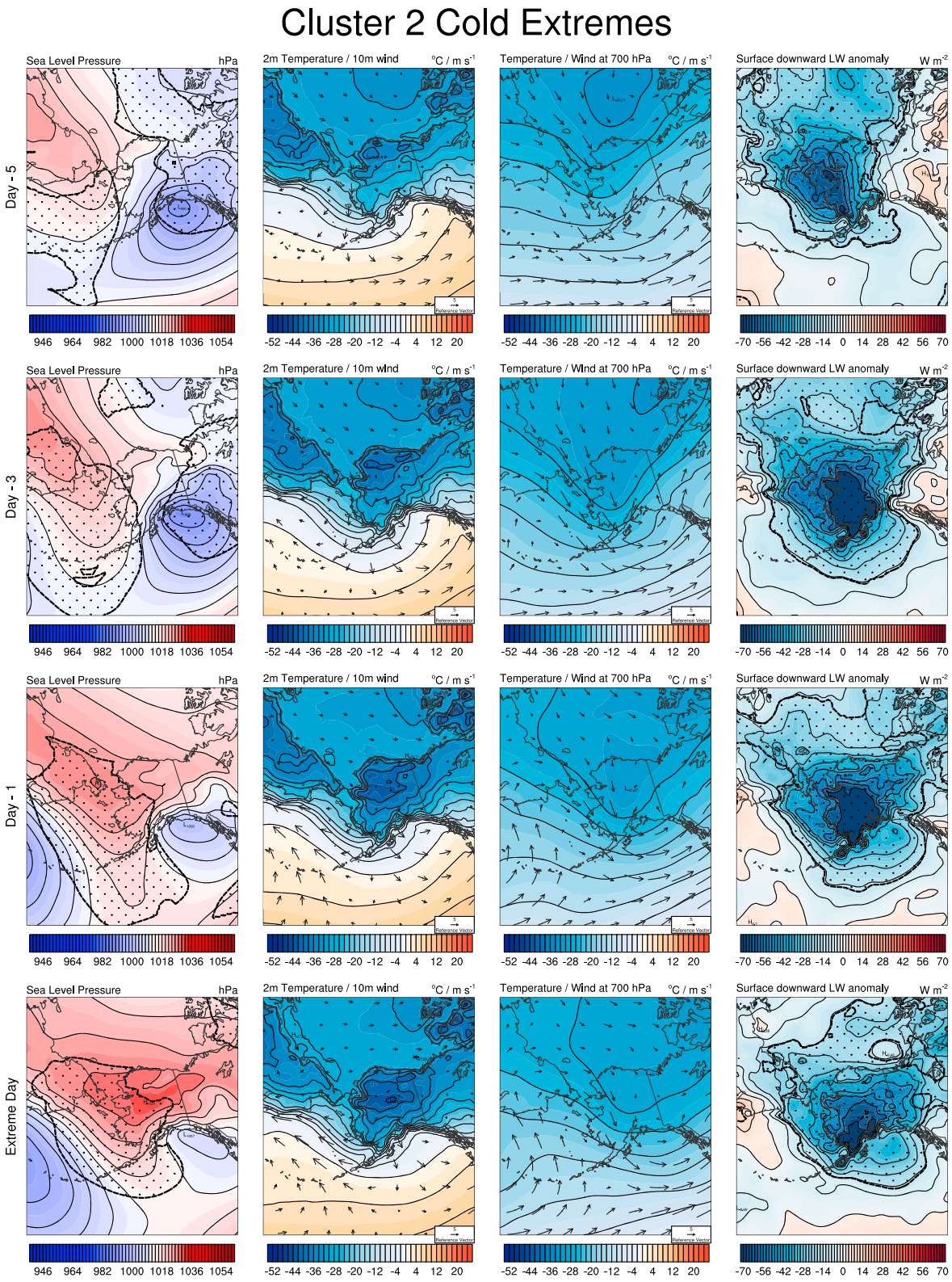

Figure 9. Composite for all widespread cold extreme days mapping to SOM cluster 2 of (first column) sea level pressure (SLP), (second column) 2 m air temperature (T2m) and 10 m wind, (third column) 700 hPa temperature (T700) and wind, and (fourth column) difference between extreme day and nonextreme day downward longwave radiation at the surface (LWD). Composites are for (first row) 5 days (day-5), (second row) 3 days (day-3), and (third row) 1 day (day-1) prior to the extreme day and the (fourth row) extreme day. Stippling indicates locations where the difference between the extreme day and nonextreme day composites differs at the 95% significance level based on a standard *t* test.

(Table 1), some of the days included in the day-5 to day-1 composites are likely to be extreme days themselves. For the 21 extreme days in cluster 2 15, 10, and 5 of the day-1, day-3, and day-5 days are also extreme days. For the 28 extremes days in cluster 5 19, 10, and 9 of the day-1, day-3, and day-5 days are extreme days.

Comparison of the cluster 5 and cluster 2 composites (Figures 8 and 9) reveals that the extreme day composite for cluster 5 (Figure 8) is similar to the day-5 composite for cluster 2 (Figure 9). In fact, 15 of the 21 day-5 days in cluster 2 map to cluster 5 (not shown). Of these 15 days that map to cluster 2 three are extreme days themselves, and this indicates that some of the extremes shown in cluster 2 represent an evolution of long events that begin as extreme days in cluster 5.

3.3.2. SOM-Based Composites of Warm Extremes

The warm extremes associated with cluster 1 account for 43.2% of all DJF warm extremes (Table 3). These extremes occur mainly in southwestern Alaska (Figure 4e). A nearly stationary surface low-pressure center located over the western Aleutian Islands strengthens between day-5 and the extreme day, while high-pressure builds over western Canada and north of Alaska (Figure 10, first column). The high-pressure center is significantly different from the nonextreme composite, while the northern edge of the low-pressure center becomes significantly different starting at day-1. The persistence of the significant differences for the high pressure over the 5 days leading up to the extreme event suggests that the high east of Alaska is most important in forcing the warm extremes. This SLP pattern drives southerly and southeasterly flow from the Pacific Ocean across Alaska, with the strongest winds over Alaska found in southwestern Alaska (Figure 10, second column).

In response to this southerly flow warm T2m moves into southwestern Alaska from the Pacific Ocean with little change in T2m over Siberia, northern Alaska, or Canada. At 700 hPa warm air is advected over Alaska in response to strong southerly flow (Figure 10, third column). The warm air at 700 hPa advances farther north than at the surface consistent with stronger advection at this height. A significant positive LWD anomaly is present over Alaska at day-5, and this anomaly strengthens through the extreme day (Figure 10, fourth column) contributing to anomalous warming of the near-surface air. The largest positive LWD anomaly occurs over western Alaska, coincident with the location of the most frequent warm extreme grid points. The positive LWD anomaly is collocated with a negative SWD anomaly (not shown) indicating that the radiative anomalies are driven by anomalous cloud cover. The increased cloud cover present for this warm extreme composite is driven by positive integrated column water vapor anomalies (not shown) and is consistent with a positive precipitation anomaly (not shown). A 500 hPa trough extending from the Chukchi Sea to the western tip of the Aleutian Islands with a ridge axis east of the largest positive LWD anomalies indicates that synoptic ascent is also likely contributing to the enhanced cloud cover for this composite.

The warm extremes associated with cluster 4 account for 39.2% of all DJF warm extremes (Table 3). These extremes occur mainly in north central and northeastern portion of the analysis domain (Figure 4f). The SLP pattern at day-5 is similar to that for cluster 1 with low pressure centered over the western Aleutian Islands and high pressure over Siberia, north of Alaska, and over western Canada (Figure 11, first column). The high-pressure centers remain relatively stationary and significantly different from the nonextreme composite for all days for the high over western Canada and for day-5 and day-3 for the high pressure over Siberia. The low-pressure center slowly drifts north toward Bering Strait while gradually weakening. From day-5 to the extreme day only the southern portion of the low-pressure center is significantly different from the nonextreme composite. At day-5 southerly surface winds over the Gulf of Alaska turn southeasterly over southern Alaska and easterly winds occur over northern Alaska (Figure 11, second column). The winds strengthen between day-5 and day-3 and then slowly weaken leading up to the extreme day. The wind direction over southern Alaska shifts from southeasterly at day-5 to nearly southerly by day-1 with southerly winds extending across all but far northern Alaska by day-1. This northward expansion of the southerly winds is consistent with the northward movement of the surface low pressure during this time period.

In response to the southerly flow which expands north across Alaska from day-5 to the extreme day warm air is advected north from the Gulf of Alaska over Alaska (Figure 11, second column). A T2m maxima in central Alaska during the extreme day may reflect downslope warming in the lee of the Alaska Range in response to the large-scale southerly flow. At 700 hPa warm air spreads north over Alaska from day-5 to the extreme day consistent with warm air advection driven by the southerly flow at this level (Figure 11, third column).

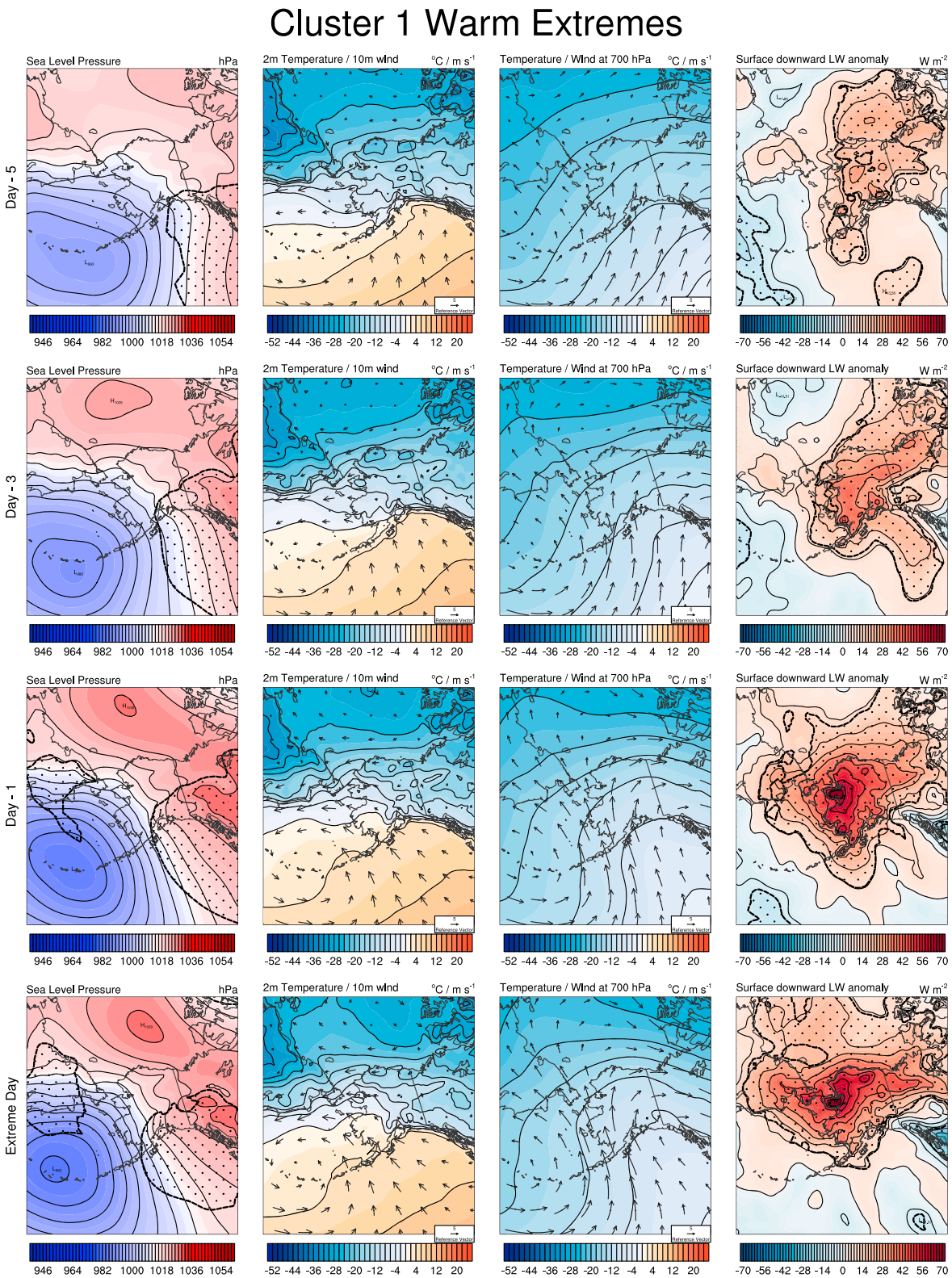

Figure 10. Composite for all widespread warm extreme days mapping to SOM cluster 1 of (first column) sea level pressure (SLP), (second column) 2 m air temperature (T2m) and 10 m wind, (third column) 700 hPa temperature (T700) and wind, and (fourth column) difference between extreme day and nonextreme day downward longwave radiation at the surface (LWD). Composites are for (first row) 5 days (day-5), (second row) 3 days (day-3), and (third row) 1 day (day-1) prior to the extreme day and the (fourth row) extreme day. Stippling indicates locations where the difference between the extreme day and nonextreme day composites differs at the 95% significance level based on a standard *t* test.

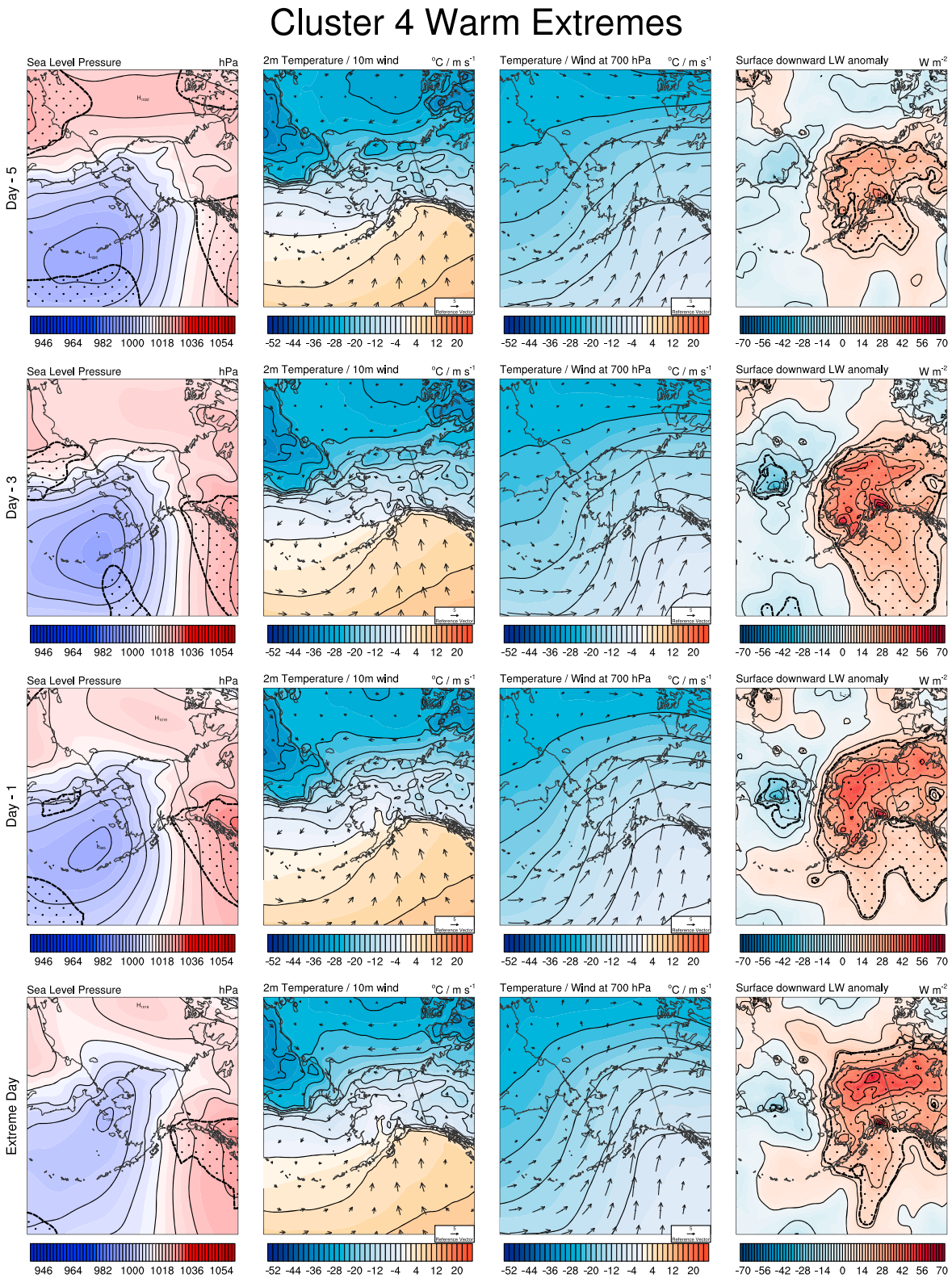

Figure 11. Composite for all widespread warm extreme days mapping to SOM cluster 4 of (first column) sea level pressure (SLP), (second column) 2 m air temperature (T2m) and 10 m wind, (third column) 700 hPa temperature (T700) and wind, and (fourth column) difference between extreme day and nonextreme day downward longwave radiation at the surface (LWD). Composites are for (first row) 5 days (day-5), (second row) 3 days (day-3), and (third row) 1 day (day-1) prior to the extreme day and the (fourth row) extreme day. Stippling indicates locations where the difference between the extreme day and nonextreme day composites differs at the 95% significance level based on a standard *t* test.

The warmest T700 is located east of the warmest air at the surface. Warming associated with a significant positive LWD anomaly occurs over Alaska for all days leading up to the extreme event (Figure 11, fourth column). The magnitude of this positive anomaly increases with time, and the largest positive anomalies are found in southwestern and central Alaska. A negative SWD anomaly (not shown) is collocated with the positive LWD anomaly indicating that the radiative anomalies are driven by anomalous cloud cover. The enhanced cloud cover for this warm extreme composite is associated with positive integrated column water vapor (not shown) and positive precipitation anomalies (not shown). A nearly stationary 500 hPa trough extending from the Chukchi Sea toward the Bering Sea with a 500 hPa ridge centered on the Alaska/Canada border places much of southern Alaska in a favorable location for synoptic scale ascent, and this may also contribute to the increased cloud cover. The difference in the location of the warmest T2m and T700 may reflect the enhanced LWD farther to the west modifying the near-surface temperature.

Comparison of the all warm extremes composite (Figure 6) with the cluster 1 (Figure 10) and cluster 4 (Figure 11) warm extreme composites highlights some similarities but several important differences. While the all warm extreme composite has warm extremes relatively evenly distributed across the analysis domain, clusters 1 and 4 composites have preferred areas of warm extreme occurrence (Figures 4d and 4f). The warm extremes occur mostly in southwestern Alaska for cluster 1 and in the north central and northeastern portion of the analysis domain in cluster 4. This difference in location of the warm extremes reflects the different evolution of the SLP field, particularly the dominant low-pressure center near the Aleutian Islands. All three SLP composites are dominated by low pressure over the Aleutian Islands and high pressure east of Alaska. The low is weaker in the all warm extreme composite, remains nearly stationary in the cluster 1 composite, and drifts north toward the Bering Strait and weakens in the cluster 4 composite. In all three warm extreme composites warm air advection is evident at both the surface and 700 hPa. The warm air spreads farther north and has maxima in central Alaska in the cluster 4 composite that is not present in the all or cluster 1 warm extreme composites. The central Alaska T2m maxima in cluster 4 may be related to downslope warming in the lee of the Alaska Range. The differences in the location of the warm extreme grid points, the different evolution of the Aleutian Low with time, and the leeside warming evident in the cluster 4 composite indicate the benefit of the SOM-based composite analysis of warm extreme events compared to the all warm extremes composite.

4. Discussion and Conclusions

The overarching goal of this research was to identify the large-scale atmospheric state associated with wintertime widespread warm and cold surface temperature extremes in southern Alaska. The warm and cold extremes were identified in daily ERA-I DJF data from 1989 to 2007 based on the coldest and warmest 1% of temperatures at each grid point in the southern Alaska analysis domain (Figure 1). Widespread extremes were defined for all days that had at least 25 warm or cold extreme grid points (Figure 4). A total of 55 widespread cold extreme days and 74 widespread warm extreme days were identified. The majority of extreme days were part of multiday events, when extremes occurred on multiple consecutive days. The cold extremes occurred as part of multiday events more frequently than warm extremes (87.3% versus 68.9%), and more cold extremes (72%) occurred as part of long (more than 4 days in duration) events than warm extremes (27%) (Table 1).

The method of self-organizing maps was used to classify all of the daily DJF SLP anomaly fields from 1989 to 2007 into 35 representative patterns (Figure 2). This SLP SOM was used to identify the SLP patterns associated with warm and cold extremes. The warm and cold extremes were found to occur in largely unique portions of the SOM space (Figure 7). The 35 SOM SLP patterns were subjectively grouped into five SOM clusters (Table 2 and Figure 2) with almost 90% of the cold and over 80% of the warm extremes associated with two of the five SOM SLP clusters (Table 3).

The warm extremes occurred with relative uniform frequency across southern Alaska (Figure 4d), while the cold extremes occurred with increased frequency from the north central to the southwestern portion of the analysis domain (Figure 4a), north and west of the high terrain of the Alaska Range (Figure 1). The preference for cold extremes in this region may reflect the shallow nature of extremely cold air masses and that these very cold air masses, which originate to the north, often cannot cross the high terrain of the Alaska Range. The preferred location of extremes differed in the different SOM clusters (Figure 4). For cluster 5

the cold extremes occurred mainly in the western portion of the analysis domain (Figure 4c), while for cluster 2 the cold extremes occurred most frequently in the central portion of the analysis domain (Figure 4b). The warm extremes were most frequent in the western portion of the analysis domain for cluster 1 (Figure 4e) and in the north central portion of the analysis domain for cluster 4 (Figure 4f).

Composites of the atmospheric state and radiative fluxes for the period from 5 days prior to each extreme day through the extreme day were created for all of the cold and warm extremes (Figures 5 and 6) and for all of the extremes in each SOM cluster (Figures 8–11). The cluster 5 cold extreme composite was characterized by high pressure over Siberia and low pressure in the Gulf of Alaska that remained relatively stationary for the 5 days leading up to the extreme. For the cluster 2 cold extreme composite (Figure 8) the Siberian high expanded over Alaska, while the Gulf of Alaska low weakened with time leading up to the extreme day. The all cold extreme composite (Figure 5) is a blend of these two cluster composites and fails to indicate the different temporal evolution evident in the cluster composites. For all three cold extreme composites cold air advection, associated with northerly flow, is stronger at 700 hPa than at the surface, and negative LWD anomalies, associated with reduced cloud cover, lead to diabatic cooling of the air near the surface. Light winds on the extreme day favor the development of strong surface inversions that enhance cooling near the surface. These results are consistent with previous work that has shown the importance of radiative cooling in the creation of cold air masses in the Arctic [*Curry*, 1983; *Turner et al*., 2013].

For the warm composites low pressure over the Aleutian Islands and high pressure centered east of Alaska are the dominant SLP features. The low pressure is weaker in the all warm extreme day composite (Figure 6), remains nearly stationary in the cluster 1 composite (Figure 10), and drifts north and weakens in the cluster 4 composite (Figure 11). Warm air advection is found in all three composites and is most pronounced at 700 hPa. The warm air spreads farthest north in the cluster 4 composite, and this composite also shows a temperature maxima north of the Alaska range that may be associated with downslope warming. Positive LWD anomalies, associated with increased cloud cover, occur over all of Alaska for all three composites, and this further increases the surface temperature.

For both warm and cold extremes both temperature advection (dominant above the surface) and anomalous LWD (positive for warm and negative for cold extremes) drive the extreme temperatures. The important role of temperature advection for both warm and cold extremes identified in this work is consistent with findings by *Loikith and Broccoli* [2012] for temperature extremes in eastern Alaska and *Cassano et al*. [2006] for temperature extremes at Barrow, Alaska. The LWD anomalies are opposite in sign to the SWD anomalies and are associated with increased (decreased) cloud cover for the warm (cold) extremes. These results are consistent with analysis of cold and warm extremes in midlatitudes that showed a combination of temperature advection and radiative effects to be important [*Kyselý*, 2008; *Andrade et al*., 2012; *Krueger et al*., 2015]. The SOM composites provide additional details regarding the large-scale atmospheric state associated with the extreme events compared to composites for all warm or cold extremes. In particular, different temporal evolution of the main low- and high-pressure centers was evident in the SOM cluster composites. The different temporal evolution led to different locations being favored for extreme events in the different clusters.

The results presented in this paper document the different atmospheric conditions that lead to widespread cold and warm extremes in southern Alaska during the winter. This work uses the same SOM and extreme days as *Cassano et al*. [2015] but differs from that work by providing a much more thorough analysis of the atmospheric state during and prior to the extreme days. *Cassano et al*. [2015] showed composite SLP patterns for extreme and nonextreme days for only two SOM patterns. Here we analyze composites of T2m and T700, 10 m and 700 hPa winds, and radiative flux anomalies for the extreme days as well as for the 5 days prior to the extreme days. These composites are created for clusters of similar SOM SLP patterns rather than for individual SOM SLP patterns, in contrast to the approach used in *Cassano et al*. [2015]. The use of SOMs to stratify the extreme days into distinct SLP patterns provides additional insight into the temporal evolution and preferred location of extremes compared to the composite analysis for all warm or cold extreme days.

As discussed in section 3.3.1, the choice to create composites relative to each extreme day rather than creating composites relative to each extreme event means that some of the prior day composites include extreme days as well. A future direction for this research would be to create composites on an event rather than a day basis.

The methods presented here are ideal for use with gridded data sets such as regional and global climate model output. Application of these techniques to future climate projections would allow for an assessment of the likelihood of changes in extreme events in response to changes in large-scale atmospheric state. Assessment of changes in Arctic extremes could also apply the method used by *Horton et al*. [2015a] to assess the role that changing circulation patterns will have on warm and cold extremes in the Arctic.

Acknowledgments
This research was funded by the United States National Science Foundation grants ARC-1023243 and ARC-1023369. We thank the four reviewers for their time and useful comments which helped improve this manuscript. ERA-Interim data were accessed from the Research Data Archive at the National Center for Atmospheric Research, Computational and Information Systems Laboratory.

References

Andrade, C., S. M. Leite, and J. A. Santos (2012), Temperature extremes in Europe: Overview of their driving atmospheric patterns, *Nat. Hazards Earth Syst. Sci.*, *12*, 1671–1691, doi:10.5194/nhess-12-1671-2012.

Cassano, E. N., A. H. Lynch, J. J. Cassano, and M. R. Koslow (2006), Classification of synoptic patterns in the western Arctic associated with extreme events at Barrow, Alaska, USA, *Climate Res.*, *30*, 83–97.

Cassano, E. N., J. J. Cassano, and M. Nolan (2011), Synoptic weather pattern controls on temperature in Alaska, *J. Geophys. Res.*, *116*, D11108, doi:10.1029/2010JD015341.

Cassano, E. N., J. M. Glisan, J. J. Cassano, W. J. Gutowski, and M. W. Seefeldt (2015), Self-organizing map analysis of widespread temperature extremes in Alaska and Canada, *Climate Res.*, *62*, 199–218, doi:10.3354/cr01274.

Curry, J. (1983), On the formation of continental polar air, *J. Atmos. Sci.*, *40*, 2278–2292.

Dee, D. P., et al. (2011), The ERA-Interim reanalysis: Configuration and performance of the data assimilation system, *Q. J. R. Meteorol. Soc.*, *137*, 553–597.

DuVivier, A. K., and J. J. Cassano (2015), Comparison of wintertime mesoscale winds over the ocean around southeastern Greenland in WRF and ERA-Interim, *Clim. Dyn.*, doi:10.1007/s00382-015-2697-8, in press.

Easterling, D. R., G. A. Meehl, C. Parmesan, S. A. Changnon, T. R. Karl, and L. O. Mearns (2000), Climate extremes: Observations, modeling, and impacts, *Science*, *289*, 2068–2074, doi:10.1126/science.289.5487.2068.

European Centre for Medium-Range Weather Forecasts (2009), Updated monthly. ERA-Interim Project. Research Data Archive at the National Center for Atmospheric Research, Computational and Information Systems Laboratory, doi:10.5065/D6CR5RD9, Accessed Oct. 2013.

Finnis, J., J. Cassano, M. Holland, M. Serreze, and P. Uotila (2009), Synoptically forced hydroclimatology of major Arctic watersheds in general circulation models. Part 1: The Mackenzie River Basin, *Int. J. Clim.*, *29*, 1226–1243.

Flato, G., et al. (2013), Evaluation of climate models, in *Climate Change 2013: The Physical Science Basis. Contribution of Working Group I to the Fifth Assessment Report of the Intergovernmental Panel on Climate Change*, edited by T. F. Stocker et al., Cambridge Univ. Press, Cambridge, U. K., and New York.

Glisan, J. M., and W. J. Gutowski Jr. (2014), WRF summer extreme daily precipitation over the CORDEX Arctic, *J. Geophys. Res. Atmos.*, *119*, 10,738–10,748, doi:10.1002/2014JD021676.

Goyette, S. (2011), Synoptic conditions of extreme windstorms over Switzerland in a changing climate, *Clim. Dyn.*, *36*, 845–866.

Grotjahn, R., et al. (2015), North American extreme temperature events and related large scale meteorological patterns: A review of statistical methods, dynamics, modeling, and trends, *Clim. Dyn.*, doi:10.1007/s00382-015-2638.

Hewitson, B. C., and R. G. Crane (2002), Self-organizing maps: Applications to synoptic climatology, *Climate Res.*, *22*, 13–26.

Horton, D. E., N. C. Johnson, D. Singh, D. L. Swain, B. Rajaratnam, and N. S. Diffenbaugh (2015a), Contribution of changes in atmospheric circulation patterns to extreme temperature trends, *Nature*, *522*, 465–469.

Horton, R. M., E. D. Coffel, J. M. Winter, and D. A. Bader (2015b), Projected changes in extreme temperature events based on the NARCCAP model suite, *Geophys. Res. Lett.*, *42*, 7722–7731, doi:10.1002/2015GL064914.

Intergovernmental Panel on Climate Change (2013), *Climate Change 2013: The Physical Science Basis. Contribution of Working Group I to the Fifth Assessment Report of the Intergovernmental Panel on Climate Change*, Cambridge Univ. Press, Cambridge, U. K.

Kohonen, T. (2001), *Self-Organizing Maps*, Springer, New York.

Krueger, O., G. C. Hegerl, and S. F. B. Tett (2015), Evaluation of mechanisms of hot and cold days in climate models over Central Europe, *Environ. Res. Lett.*, *10*, 014002, doi:10.1088/1748-9326/10/1/014002.

Kyselý, J. (2008), Influence of the persistence of circulation patterns on warm and cold temperature anomalies in Europe: Analysis over the 20th century, *Global Planet. Change*, *62*, 147–163.

Leloup, J., M. Lengaigne, and J.-P. Boulanger (2008), Twentieth century ENSO characteristics in the IPCC database, *Clim. Dyn.*, *30*, 277–291.

Leloup, J. A., Z. Lachkar, J.-P. Boulanger, and S. Thiria (2007), Detecting decadal changes in ENSO using neural networks, *Clim. Dyn.*, *28*, 147–162.

Lennard, C., and G. Hegerl (2015), Relating changes in synoptic circulation to the surface rainfall response using self-organising maps, *Clim. Dyn.*, *44*, 861–879.

Lindsay, R., M. Wensnahan, A. Schweiger, and J. Zhang (2014), Evaluation of seven different atmospheric reanalysis products in the arctic, *J. Clim.*, *27*, 2588–2606, doi:10.1175/JCLI-D-13-00014.1.

Loikith, P. C., and A. J. Broccoli (2012), Characteristics of observed atmospheric circulation patterns associated with temperature extremes over North America, *J. Clim.*, *25*, 7266–7281, doi:10.1175/JCLI-D-11-00709.1.

Loikith, P. C., and A. J. Broccoli (2015), Comparison between observed and model-simulated atmospheric circulation patterns associated with extreme temperature days over North America using CMIP5 historical simulations, *J. Clim.*, *28*, 2063–2079, doi:10.1175/JCLI-D-13-00544.1.

Meehl, G. A., C. Tebaldi, G. Walton, D. Easterling, and L. McDaniel (2009), Relative increase of record high maximum temperatures compared to record low minimum temperatures in the U.S., *Geophys. Res. Lett.*, *36*, L23701, doi:10.1029/2009GL040736.

Metz, N. D., H. M. Archambault, A. F. Srock, T. J. Galameau, and L. F. Bosart (2013), A comparison of South American and African preferential pathways for extreme cold events, *Mon. Weather Rev.*, *141*, 2066–2086.

Mills, C. M., and J. E. Walsh (2014), Synoptic activity associated with sea ice variability in the Arctic, *J. Geophys. Res. Atmos.*, *119*, 12,117–12,131, doi:10.1002/2014JD021604.

Mohr, M. (2004), Problems with the mean sea level pressure field over the western United States, *Mon. Weather Rev.*, *132*, 1952–1965.

Nigro, M. A., and J. J. Cassano (2014a), Identification of surface wind patterns over the Ross Ice Shelf, Antarctica, using self organizing maps, *Mon. Weather Rev.*, *142*, 2361–2378, doi:10.1175/MWR-D-13-00382.1.

Nigro, M. A., and J. J. Cassano (2014b), Analysis of the Ross Ice Shelf airstream forcing mechanisms using self organizing maps, *Mon. Weather Rev.*, *142*, 4719–4734, doi:10.1175/MWR-D-14-00077-1.

Ning, L., and R. S. Bradley (2015), Winter climate extremes over the northeastern United States and southeastern Canada and teleconnections with large-scale modes of climate variability, *J. Clim.*, *28*, 2475–2493, doi:10.1175/JCLI-D-13-00750.1.

Ning, L., E. E. Riddle, and R. S. Bradley (2015), Projected changes in climate extremes over the northeastern United States, *J. Clim.*, *28*, 3289–3310, doi:10.1175/JCLI-D-14-00150.1.

Randall, D. A., et al. (2007), Climate models and their evaluation, in *Climate Change 2007: The Physical Science Basis. Contribution of Working Group I to the Fourth Assessment Report of the Intergovernmental Panel on Climate Change*, edited by S. Solomon et al., Cambridge Univ. Press, Cambridge, U. K., and New York.

Rodríguez-Puebla, C., A. H. Encinas, L. A. García-Casado, and S. Nieto (2010), Trends in warm days and cold nights over the Iberian Peninsula: Relationships to large-scale variables, *Clim. Change*, *100*, 667–684.

Screen, J. A., and I. Simmonds (2010), The central role of diminishing sea ice in recent Arctic temperature amplification, *Nature*, *464*, 1334–1337.

Seefeldt, M. W., and J. J. Cassano (2012), A description of the Ross Ice Shelf air stream (RAS) through the use of self-organizing maps (SOMs), *J. Geophys. Res.*, *117*, D09112, doi:10.1029/2011JD016857.

Serreze, M. C., and J. A. Francis (2006), The Arctic amplification debate, *Clim. Change*, *76*, 241–264, doi:10.1007/s10584-005-9017-y.

Serreze, M. C., A. P. Barrett, J. C. Stroeve, D. N. Kindig, and M. M. Holland (2009), The emergence of surface-based Arctic amplification, *Cryosphere*, *3*, 11–19.

Shan, H., Y. Guan, and J. Huang (2014), Surface air temperature patterns on a decadal scale in China using self-organizing map and their relationship to Indo-Pacific warm pool, *Int. J. Clim.*, *34*, 3752–3765.

Sheridan, S. C., and C. C. Lee (2011), The self-organizing map in synoptic climatological research, *Prog. Phys. Geogr.*, *35*, 109–119.

Stefanon, M., F. D'Andrea, and P. Drobinski (2012), Heatwave classification over Europe and the Mediterranean region, *Environ. Res. Lett.*, *7*, 014023, doi:10.1088/1748-9326/7/1/014023.

Tebaldi, C., K. Hayhoe, J. M. Arblaster, and G. A. Meehl (2006), Going to the extremes: An intercomparison of model-simulated historical and future changes in extreme events, *Clim. Change*, *79*, 185–211, doi:10.1007/s10584-006-9051-4.

Turner, J. K., J. Gyakum, and S. M. Milrad (2013), A thermodynamic analysis of an intense North American Arctic air mass, *Mon. Weather Rev.*, *141*, 166–181, doi:10.1175/MWR-D-12-00176.1.

Wallace, J. M., and P. V. Hobbs (1977), *Atmospheric Science: An Introductory Survey*, Academic Press, Inc, San Diego, Calif.